Structural Engineering and Mechanics, *Vol. 69, No. 1 (2019) 33-42*
DOI: https://doi.org/10.12989/sem.2019.69.1.033

Incremental extended finite element method for thermal cracking of mass concrete at early ages

Zhenyang Zhu*, Guoxin Zhang[a], Yi Liu[a] and Zhenhong Wang[a]

State Key Laboratory of Simulation and Regulation of Water Cycle in River Basin, China Institute of Water Resources and Hydropower Research, Beijing 100038, P.R. China

(Received March 6, 2018, Revised November 15, 2018, Accepted November 16, 2018)

Abstract. Thermal cracks are cracks that commonly form at early ages in mass concrete. During the concrete pouring process, the elastic modulus changes continuously. This requires the time domain to be divided into several steps in order to solve for the temperature, stress, and displacement of the concrete. Numerical simulations of thermal crack propagation in concrete are more difficult at early ages. To solve this problem, this study divides crack propagation in concrete at early ages into two cases: the case in which cracks do not propagate but the elastic modulus of the concrete changes and the case in which cracks propagate at a certain time. This paper provides computational models for these two cases by integrating the characteristics of the extended finite element algorithm, compiles the corresponding computational programs, and verifies the accuracy of the proposed model using numerical comparisons. The model presented in this paper has the advantages of high computational accuracy and stable results in resolving thermal cracking and its propagation in concrete at early ages.

Keywords: thermal crack; extended finite element; propagation; concrete; early age

1. Introduction

Thermal cracks are cracks that commonly form at early ages in mass concrete. Research on thermal cracks includes studies of thermal stress calculations, temperature fields, and thermal crack propagation in concrete (Zhu 2010).

Many studies have investigated temperature and stress fields of early-age mass concrete. Waller and Cussigh (2004) studied the maturity level of concrete due to the application of thermal stress at an early age. Schutter (2002) studied early-age thermal stresses in mass concrete based on hydration. Zhu and Chen (2017) performed research on concrete hydration and used the results to study the thermodynamic properties of concrete. Wang and Navi (1997) studied the mechanical properties of early-age concrete in a project structure. Zhu and Qiang (2013) presented an equivalent algorithm and discrete iterative algorithm for mass concrete containing a water pipe. Kim (2001) developed a temperature field algorithm for mass concrete containing a water pipe based on the principle of thermal equilibrium and the linear element method. Wang and Yan (2013) developed an algorithm to evaluate early age mechanical properties of concrete.

These investigations mainly studied the temperature and stress fields in concrete. Because stress is not the direct cause of crack propagation and the conventional finite element method cannot predict the condition of concrete after the development of cracks, fracture mechanics is required to study the propagation of thermal cracks in early-age concrete.

Many studies have focused on numerical simulation methods of fracturing in concrete, such as the embedded finite element method (EFEM) (Linder and Armero 2007, Linder and Armero 2009, Dvorkin and Cuitino 2010), meshfree methods (MMs) (Belytschko and Lu 1994, Liu and Jun 1995, Atluri 2002, Bordas and Rabczuk 2008), and boundary element methods (BEMs) (Aliabadi 1997, Pan and Yuan 2000, Sfantos and Aliabadi 2007, Simpson and Bordas 2012). The extended finite element method (XFEM) was first proposed by the research group of Prof. Belytschko and Prof. Moes at Northwestern University in the United States in 1999 and has since been significantly extended (Belytschko and Black, 1999, Moës and Dolvow 1999, Stolarska and Chopp 2016, Belytschko and Chen 2003). Crack propagation is calculated using XFEM, and remeshing is not conducted during the crack propagation process. XFEM has several advantages over the conventional finite element method and is widely used in crack propagation analyses. XFEM has attracted increasing attention and has been widely used in many fields of numerical simulation (Zuo and Hu 2015, Himanshu and Akhilendra 2012, Jiang and Tay 2013, Liu and Hu 2013, Elena 2014, Jrad 2018).

The elastic modulus of mass concrete changes during the pouring process. Therefore, calculations of the thermal stress and displacement require the use of incremental methods, i.e., the time domain must be divided into several steps, and the solutions must be calculated in each step to obtain the total displacement and stress of the structure. For early-age concrete, the displacement and stress can be obtained accurately only by using the incremental method. However, taking crack propagation into account using the

*Corresponding author, Professor
E-mail: 1219921552@qq.com
[a]Ph.D.

http://www.techno-press.com/journals/sem&subpage=7
ISSN: 1225-4568 (Print), 1598-6217 (Online)

incremental method is difficult. For this reason, this paper presents the incremental XFEM method to address the thermal stress problem of early-age concrete.

2. Basic principle of analysis

2.1 Basic principle of XFEM

T Belytschko et al. proposed XFEM for analyzing cracking problems. To reconstruct the displacement in the region around the crack surface, the idea of a partition of unity was applied to strengthen the nodes around the discontinuous surface using an additional function, which reflects the discontinuity of the crack surface. By further developing the extended finite element, the description of the displacement is improved continuously, and the accuracy and convergence speed are also enhanced. This paper introduces the extended finite element displacement mode that was employed in this paper (Belytschko and Black, 1999, Moës and Dolvow 1999, Stolarska and Chopp 2016, Belytschko and Chen 2003).

The elements that are penetrated by cracks are enhanced by the discontinuous general Heaviside function (Fig. 1; the hollow circles represent nodes). The element that contains a crack tip is enhanced through the application of a crack tip progressive displacement field function (Fig. 2; the solid circles represent nodes) to reflect the local characteristics of the crack tip region. The additional function can indirectly reflect the existence of a crack surface. Thus, when the finite element mesh is divided, the crack surface and the finite element mesh can be independent of each other. The crack surface can be located anywhere on the grid, which overcomes the difficulties associated with high-density grids in regions of high stress and concentrated deformation, such as a crack tip. When simulating crack propagation, remeshing is not necessary. The outer-layer elements surrounding the crack tip element can be enhanced to ensure computational accuracy, as shown in Fig. 2.

The displacement mode of the extended finite element can be expressed as

$$u(x)=\sum_{j=1}^{n}N_j(x)u_j+\sum_{h=1}^{mh}N_h(x)\left[H(x)-H(x_h)\right]a_h \\ +\sum_{k=1}^{mt}N_k(x)\sum_{l=1}^{4}\left\{\left[F_l(x)-F_l(x_k)\right]b_k^l\right\} \tag{1}$$

where n is the number of conventional element nodes, $N_j(x)$ is the shape function, u_j is the degree of freedom vector for a conventional finite element node, m_h is the number of enhanced nodes on both sides of the crack surface, $H(x)$ is the value of the Heaviside function at the Gaussian point x, $H(x_h)$ is the value of the Heaviside function at point h, a_h is the degree of freedom vector of the enhanced node on both sides of the crack surface, mt is the number of enhanced nodes at the crack tip, $F_l(x)$ is the value of the crack tip enhancement function at the Gaussian point x, $F_l(x_k)$ is the value of the crack tip enhancement function at the enhancement node, and b_k^l is

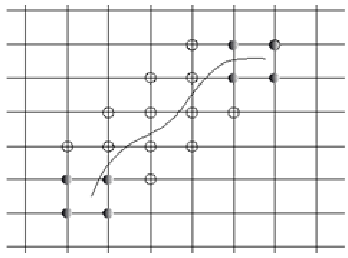

Fig. 1 A crack located on a grid

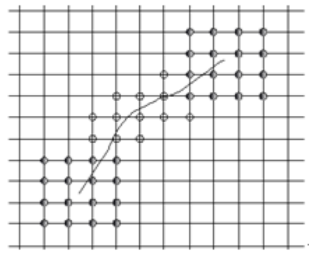

Fig. 2 Enhancement of the crack tip element nodes

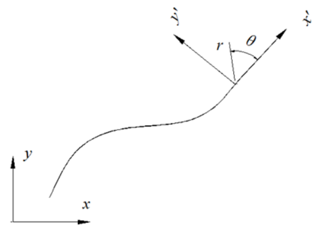

Fig. 3 Local crack tip coordinate system

the degree of freedom vector for the enhanced node at the crack tip.

By dividing the crack into two sides, the Heaviside enhancement function $H(x)$, which is 1 on one side of the crack and –1 on the other side, is expressed mathematically as follows

$$H(x)=\begin{cases}1 & (x-x^*)n\geq 0\\ -1 & (x-x^*)n<0\end{cases} \tag{2}$$

where x is the point that is examined, x^* is the point on the crack surface closest to x, and n is the unit outer normal vector of the crack at x^*.

F_l is the crack tip enhancement function, which is a set of linearly independent bases that was extracted from the analytical expression of the crack tip displacement field from linear elastic fracture mechanics. When defined in the polar coordinate system at the crack tip, the expression of each material term in the same row is

$$\{F_l(r,\theta)\}_{l=1}^{4}=\left\{\sqrt{r}\sin\frac{\theta}{2},\sqrt{r}\cos\frac{\theta}{2},\sqrt{r}\sin\theta\sin\frac{\theta}{2},\sqrt{r}\sin\theta\cos\frac{\theta}{2}\right\} \tag{3}$$

where r and θ are expressed as polar coordinates in the local crack tip coordinate system, as shown in Fig. 3.

Eqs. (1) to (3) are the basic displacement format of the extended finite element that was applied in this study.

Although the integration method for the stiffness matrix and the overall stiffness matrix of the extended finite element are more complicated, in principle, they are not different from that of the conventional finite element.

2.2 Calculation method for the thermal stress field of mass concrete

During the concrete hardening process, the elastic modulus changes continuously. By taking changes in the elastic modulus into account, accurate solutions can be found for the stress and strain during the hardening of mass concrete. The thermal stress field of mass concrete is similar to the linear elastic stress field, which can be solved using only the incremental method; therefore, the stress and displacement of concrete can be accurately calculated. The calculation method for the thermal stress field of mass concrete is described below (Zhu 1998).

The calculation time is divided into m periods. The thermal strain increment generated during period Δt_m is

$$\left\{\Delta\varepsilon_m^T\right\} = \{\varepsilon(t_m)\} - \{\varepsilon(t_{m-1})\} \tag{4}$$

where $\left\{\Delta\varepsilon_m^T\right\}$ is the thermal strain increment.

In the finite element calculation, the stiffness matrix of the element can be expressed as

$$[k]^e = \iint [B]^T [D_m][B] dxdy \tag{5}$$

where the matrix $[B]$ is the strain matrix of the element, and $[D_m]$ is the elastic matrix of the element.

The element load increment induced by a two-dimensional finite-element non-stress deformation can be expressed as

$$\left[\Delta P_m\right]_e^T = \iint [B]^T [D_m]\left[\Delta\varepsilon_m^T\right] dxdy \tag{6}$$

where $\left[\Delta P_m\right]_e^T$ is the element node load increment caused by temperature.

The nodal force and nodal load are combined to obtain the overall equilibrium equation

$$[K]\{\Delta\delta_m\} = \left[\Delta P_m\right]^T \tag{7}$$

where $\left[\Delta P_m\right]^T$ is the node load increment caused by temperature.

2.3 Integration method for the stress intensity factors

A previous study (Herrmann 1981) described the energy integral method that solves the stress intensity factors in detail.

The crack tip is set as the origin and the tangent to the crack surface as the x_1 axis of the local polar coordinate system. In terms of the composite loading mode, the relation between the J integral and the stress intensity factors is

$$J = \frac{K_{\mathrm{I}}^2}{E^*} + \frac{K_{\mathrm{II}}^2}{E^*} \tag{8}$$

where E^* is related to the Young's modulus E and Poisson's ratio ν, $E^* = E$ (plane stress), $E^* = \dfrac{E}{1-\nu^2}$ (plane strain), and K_{I} and K_{II} are type I and II stress intensity factors, respectively.

Two stress states are considered: state 1 $(\sigma_{ij}^{(1)}, \varepsilon_{ij}^{(1)}, u_{ij}^{(1)})$ is the real state, and state 2 $(\sigma_{ij}^{(2)}, \varepsilon_{ij}^{(2)}, u_{ij}^{(2)})$ is the auxiliary state. If state 2 is set as the progressive field, then the J integral of the sum of the two states is

$$J^{(1+2)} = \int_\Gamma \left[\frac{1}{2}(\sigma_{ij}^{(1)} + \sigma_{ij}^{(2)})(\varepsilon_{ij}^{(1)} + \varepsilon_{ij}^{(2)})\delta_{ij} - (\sigma_{ij}^{(1)} + \sigma_{ij}^{(2)})\frac{\partial(u_i^{(1)} + u_j^{(2)})}{\partial x_1}\right] n_j d\Gamma \tag{9}$$

Rearranging this equation gives

$$J^{(1+2)} = J^{(1)} + J^{(2)} + M^{(1+2)} \tag{10}$$

where $M^{(1+2)}$ is called the mutual integral of states 1 and 2, which is

$$M^{(1+2)} = \int_\Gamma \left[W^{(1,2)}\delta_{1j} - \sigma_{ij}^{(1)}\frac{\partial u_i^{(2)}}{\partial x_1} - \sigma_{ij}^{(2)}\frac{\partial u_i^{(1)}}{\partial x_1}\right] n_j d\Gamma \tag{11}$$

where $M^{(1+2)}$ is the interactive strain energy

$$M^{(1+2)} = \sigma_{ij}^{(1)}\varepsilon_{ij}^{(2)} = \sigma_{ij}^{(2)}\varepsilon_{ij}^{(1)} \tag{12}$$

Eq. (12) can be written as

$$J^{(1+2)} = J^{(1)} + J^{(2)} + \frac{2}{E^*}(K_{\mathrm{I}}^{(1)}K_{\mathrm{I}}^{(2)} + K_{\mathrm{II}}^{(1)}K_{\mathrm{II}}^{(2)}) \tag{13}$$

Combining Eq. (10) with Eq. (13) gives

$$M^{(1+2)} = \frac{2}{E^*}(K_{\mathrm{I}}^{(1)}K_{\mathrm{I}}^{(2)} + K_{\mathrm{II}}^{(1)}K_{\mathrm{II}}^{(2)}) \tag{14}$$

State 2 is set as the progressive field of the type I stress intensity factor. In addition, $K_{\mathrm{I}}^{(2)} = 1$, $K_{\mathrm{II}}^{(2)} = 0$, which gives the type I stress intensity factor for state 1

$$K_{\mathrm{I}}^{(1)} = \frac{E^*}{2} M^{(1,\ \text{mode I})} \tag{15}$$

State 2 is set as the progressive field of the type II stress intensity factor. $K_{\mathrm{I}}^{(2)} = 0$ and $K_{\mathrm{II}}^{(2)} = 1$, which gives the type II stress intensity factor for state 1

$$K_{\mathrm{II}}^{(1)} = \frac{E^*}{2} M^{(1,\ \text{mode II})} \tag{16}$$

The contour integral (11) can be rewritten as

$$M^{(1+2)} = \int_C \left[W^{(1,2)}\delta_{1j} - \sigma_{ij}^{(1)}\frac{\partial u_i^{(2)}}{\partial x_1} - \sigma_{ij}^{(2)}\frac{\partial u_i^{(1)}}{\partial x_1}\right] q m_j d\Gamma \tag{17}$$

where $C = \Gamma + C_+ + C_- + \Gamma_0$, and m_j is the unit outer normal vector of the contour C. According to Green's formula, Eq. (18) can be rewritten in integral form on area A

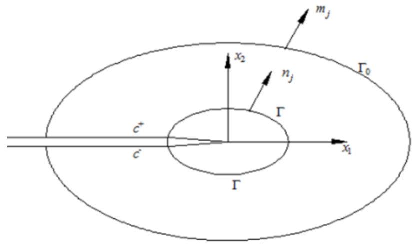

Fig. 4 Mutual integration diagram

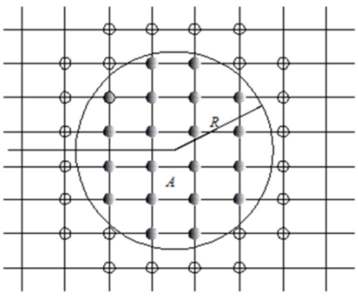

Fig. 5 M integral element selection and node integral weight around the crack tip

$$M^{(1+2)} = \int_A \left[\sigma_{ij}^{(1)} \frac{\partial u_i^{(2)}}{\partial x_1} + \sigma_{ij}^{(2)} \frac{\partial u_i^{(1)}}{\partial x_1} - W^{(1,2)} \delta_{1j} \right] \frac{\partial q}{\partial x_j} dA \tag{18}$$

In Eq. (18), state 1 is selected as the true state of the problem, to which the finite element solution applies. State 2 is the progressive solution of the crack tip denoted by aux, and Eq. (18) can be further expanded

$$\begin{aligned} M^{(1+2)} = \int_A \Bigg[& \left(\sigma_x \frac{\partial u_x^{aux}}{\partial x} + \tau_{xy} \frac{\partial u_y^{aux}}{\partial x} \sigma_x^{aux} \frac{\partial u_x}{\partial x} + \tau_{xy}^{aux} \frac{\partial u_y}{\partial x} - \sigma_{ij} \varepsilon_{ij}^{aux} \right) \frac{\partial q}{\partial x} \\ & + \left(\tau_{xy} \frac{\partial u_x^{aux}}{\partial x} + \sigma_y \frac{\partial u_y^{aux}}{\partial x} \tau_{xy}^{aux} \frac{\partial u_x}{\partial x} + \sigma_y^{aux} \frac{\partial u_y}{\partial x} \right) \frac{\partial q}{\partial y} \Bigg] dA \end{aligned} \tag{19}$$

Region A is shown in Fig. 4. In Eq. (19), q is defined as the weight function, q is 1 (solid point in Fig. 5) when the node is within the integration region A, and q is 0 (hollow point in Fig. 5) when the node is outside the integration region A. The inserted value through the element node at an arbitrary point q of the element is $q = \sum_{i=1}^{4} N_i q_i$.

2.4 Integration method for the stress intensity factors

According to the basic principles of linear elastic fracture mechanics, the displacement field, strain field and stress field that are caused by the linear elastic stress near the crack tip can be calculated as follows (Sneddon 1946).

If $K_{\mathrm{I}}^{\mathrm{aux}} = 1$ and $K_{\mathrm{II}}^{\mathrm{aux}} = 0$

$$u_{\text{mode I}} = \begin{cases} u_x^{aux} = \dfrac{1}{2G} \sqrt{\dfrac{r}{2\pi}} \left[(\kappa - 1)\cos\dfrac{\theta}{2} + \sin\dfrac{\theta}{2}\sin\theta \right] \\ u_y^{aux} = \dfrac{1}{2G} \sqrt{\dfrac{r}{2\pi}} \left[(\kappa + 1)\sin\dfrac{\theta}{2} - \cos\dfrac{\theta}{2}\sin\theta \right] \end{cases} \tag{20}$$

If $K_{\mathrm{I}}^{\mathrm{aux}} = 0$ and $K_{\mathrm{II}}^{\mathrm{aux}} = 1$

$$u_{\text{mode II}} = \begin{cases} u_x^{aux} = \dfrac{1}{2G} \sqrt{\dfrac{r}{2\pi}} \left[(\kappa + 1)\sin\dfrac{\theta}{2} + \cos\dfrac{\theta}{2}\sin\theta \right] \\ u_y^{aux} = \dfrac{1}{2G} \sqrt{\dfrac{r}{2\pi}} \left[-(\kappa - 1)\cos\dfrac{\theta}{2} + \sin\dfrac{\theta}{2}\sin\theta \right] \end{cases} \tag{21}$$

where $\kappa = 3\text{-}4\nu$ (plane strain), $\kappa = \dfrac{3\text{-}\nu}{1+\nu}$ (plane stress), and $G = \dfrac{E}{2(1+\nu)}$.

$$\frac{u_x^{aux}}{\partial x} = \frac{u_x^{aux}}{\partial r}\frac{\partial r}{\partial x} + \frac{u_x^{aux}}{\partial \theta}\frac{\partial \theta}{\partial x}, \frac{u_y^{aux}}{\partial x} = \frac{u_y^{aux}}{\partial r}\frac{\partial r}{\partial x} + \frac{u_y^{aux}}{\partial \theta}\frac{\partial \theta}{\partial x} \tag{22}$$

$$\frac{u_x^{aux}}{\partial y} = \frac{u_x^{aux}}{\partial r}\frac{\partial r}{\partial y} + \frac{u_x^{aux}}{\partial \theta}\frac{\partial \theta}{\partial y}, \ \frac{u_y^{aux}}{\partial y} = \frac{u_y^{aux}}{\partial r}\frac{\partial r}{\partial y} + \frac{u_y^{aux}}{\partial \theta}\frac{\partial \theta}{\partial y} \tag{23}$$

If $K_{\mathrm{I}}^{\mathrm{aux}} = 1$ and $K_{\mathrm{II}}^{\mathrm{aux}} = 0$

$$\sigma_{\text{mode I}} = \begin{cases} \sigma_x^{aux} = \dfrac{1}{\sqrt{2\pi r}} \cos\dfrac{\theta}{2} (1 - \sin\dfrac{\theta}{2}\sin\dfrac{3\theta}{2}) \\ \sigma_y^{aux} = \dfrac{1}{\sqrt{2\pi r}} \cos\dfrac{\theta}{2} (1 + \sin\dfrac{\theta}{2}\sin\dfrac{3\theta}{2}) \\ \tau_{xy}^{aux} = \dfrac{1}{\sqrt{2\pi r}} \cos\dfrac{\theta}{2} \sin\dfrac{\theta}{2} \cos\dfrac{3\theta}{2} \end{cases} \tag{24}$$

If $K_{\mathrm{I}}^{\mathrm{aux}} = 0$ and $K_{\mathrm{II}}^{\mathrm{aux}} = 1$

$$\sigma_{\text{mode II}} = \begin{cases} \sigma_x = -\dfrac{1}{\sqrt{2\pi r}} \sin\dfrac{\theta}{2} (2 + \cos\dfrac{\theta}{2}\cos\dfrac{3\theta}{2}) \\ \sigma_y = \dfrac{1}{\sqrt{2\pi r}} \sin\dfrac{\theta}{2} \cos\dfrac{\theta}{2} \cos\dfrac{3\theta}{2} \\ \tau_{xy} = \dfrac{1}{\sqrt{2\pi r}} \cos\dfrac{\theta}{2} (1 - \sin\dfrac{\theta}{2}\sin\dfrac{3\theta}{2}) \end{cases} \tag{25}$$

3. Temperature load extended finite element

3.1 The extended finite element-incremental method

For early-age concrete, factors such as the change of elastic modulus and creep should be considered, and the incremental method is required to solve for the displacement and stress caused by the temperature load and autogenous deformation.

As shown in Fig. 6, the crack propagation is divided into n steps, and the displacement and stress of the structure after the n^{th} crack propagation can be expressed as

$$\begin{cases} u_{n+1} = u_n + \Delta u_n \\ \sigma_{n+1} = \sigma_n + \Delta \sigma_n \end{cases} \tag{26}$$

where u_n is the initial displacement of crack propagation at the n^{th} step, Δu_n is the displacement increment after a

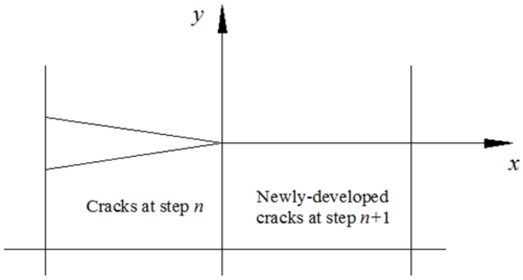

Fig. 6 Plane propagation of cracks

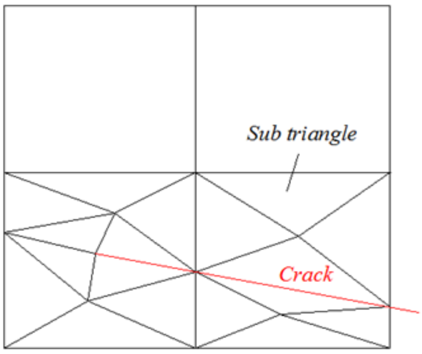

Fig. 7 Sub-element division of a crack

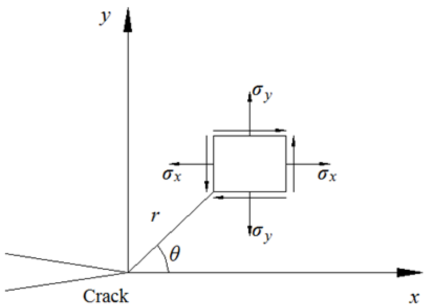

Fig. 8 Stress element in a planar problem

stress of the same magnitude but in the opposite direction is applied to the new crack surface, σ_n is the initial stress of the crack propagation at the n^{th} step, and $\Delta\sigma_n$ is the stress increment after a stress of the same magnitude but in the opposite direction is applied to the new crack surface.

3.2 Loading mode of newly developed surface stress

The extended finite element can be divided into crack tip elements, crack elements and conventional elements. As shown in Fig. 7, when solving for structural crack propagation using the extended finite element, the element in which the crack is located can be divided into several sub-elements, which are used to arrange the integration points. When calculating crack propagation using the incremental method, the newly developed crack surface should experience a stress of the same magnitude but in the opposite direction. The specific implementation methods include the stress method based on an integration point near the newly developed crack surface and the progressive field analytical solution fitting method. Considering the error that exists in the extended finite element, if the mesh is sufficiently detailed, the analytical solution can be used to perform the fitting to obtain higher calculation accuracy.

In Fig. 8, the crack represents the origin of the coordinate system, the x-direction is the direction in which the crack propagates, and the y-direction is normal to the crack surface. In the case that the stress intensity factor is known, an infinitely flat plate containing type I and II composite cracks is subjected to a uniform load. According to linear elastic fracture mechanics, the stress near the crack tip can be written as follows

$$\sigma_{\text{n}} = K_{\text{I, n}}\sigma_{\text{mode I, n}} + K_{\text{II, n}}\sigma_{\text{mode II, n}} \tag{27}$$

The meaning of each parameter in the formula is the same as in Section 2.4.

As shown in Fig. 8, $\theta = 0$ is the direction in which the crack propagates. According to Eq. (27), if $\theta = 0$, the stress distribution on the crack surface prior to crack propagation can be obtained

$$\begin{cases} \sigma_x = \sigma_y = \dfrac{K_{\text{I}}}{\sqrt{2\pi r}} \\ \tau_{xy} = \dfrac{K_{\text{II}}}{\sqrt{2\pi r}} \end{cases} \tag{28}$$

When calculating the stress and displacement in step n+1 by means of the extended finite element-incremental method, stress should be exerted on the newly developed crack surface; that is, a stress of the same magnitude but in the opposite direction is applied to the newly formed crack surface. The extended finite element loading mode is the same as that in the finite element. In the conventional units of the extended finite element, there are two degrees of freedom for the node load; for crack-penetrated elements, the node load has 4 degrees of freedom. For the elements in which the crack tip is located, the node load has 10 or 12 degrees of freedom. The degrees of freedom for the extended finite element node load can be expressed as

$$\{F\}^{\text{e}} = \begin{cases} \{F_{1,1},\ F_{1,2},\ F_{2,1},\ F_{2,2},\cdots F_{n,i}\cdots\}^{\text{T}} & CE \\ \{F_{1,1},\ F_{1,2},\ F_{1,3},F_{1,4},\ F_{2,1},\ F_{2,2},\ F_{2,3},F_{2,3},\cdots F_{n,i}\cdots\}^{\text{T}} & CPE \\ \{F_{1,1},\ F_{1,2},\ F_{1,3},F_{1,4}\cdots,F_{1,10},\cdots F_{n,i}\cdots\}^{\text{T}} & CTE \end{cases} \tag{29}$$

where *CE* is a conventional element, *CPE* is a crack-penetrated element, and *CTE* is a crack tip element.

The loading method given in Eq. (29) is similar to that for the hydraulic fracturing load on cracks. A detailed derivation of the relevant loading method is given in a previous report (Dong and Ren 2011).

3.3 Stress-strain and M-integral methods of hardened concrete in the case of a non-propagated crack

The time domain is divided into m periods. The elastic strain caused by thermal load in the m^{th} period can be obtained by

$$\{\Delta\varepsilon_m^e\} = \{\Delta\varepsilon_m\} - \{\Delta\varepsilon_m^T\} \tag{30}$$

where $\{\Delta\varepsilon_m^e\}$ is elastic strain and $\{\Delta\varepsilon_m\}$ is the strain

calculated by Eq. (7).
and the elastic stress satisfies

$$\left\{\Delta\sigma_m^e\right\} = \left[D\right]\left\{\Delta\varepsilon_m^e\right\} \tag{31}$$

The elastic stress at the end of the m^{th} period can be expressed as

$$\sigma_{m+1} = \sigma_m + \Delta\sigma_m \tag{32}$$

where σ_m is the initial elastic stress in the m^{th} period, and $\Delta\sigma_m$ is the thermal stress increment in the m^{th} period.

Because the concrete elastic modulus changes in the m^{th} step, based on the relation between the elastic stress and the elastic strain, the elastic strain that forms at the end of period m due to the elastic stress can be expressed by the following formula

$$\varepsilon_{m+1}^e = \frac{E_m}{E_{m+1}}\varepsilon_m^e + \Delta\varepsilon_m^e \tag{33}$$

where E_m represents the initial elastic modulus of the concrete in the m^{th} period, E_{m+1} represents the initial elastic modulus of the concrete in period m+1 (i.e., the elastic modulus of the concrete at the end of period m), ε_m^e is the initial elastic strain in the m^{th} period, and $\Delta\varepsilon_m^e$ is the elastic strain increment in the m^{th} period.

3.4 Calculation methods for the concrete stress and strain in the case of crack propagation

The extended finite element can be divided into conventional elements, crack-penetrated elements and crack tip elements. During crack propagation, if the type of element does not change, then the position of the integration point within the element will not change. At this point, the stress (or strain) of the integration point prior to crack propagation together with the newly developed stress and strain are briefly superimposed, and the stress (or strain) after crack propagation is given. The relation between the stress and the strain before and after crack propagation can be expressed as follows.

For elements whose integration point does not change before and after crack propagation, the stress after the n^{th} propagation is

$$\sigma_{n+1} = \sigma_n + \Delta\sigma_n \tag{34}$$

where σ_n is the initial stress at the n^{th} propagation, and $\Delta\sigma_n$ is the stress increment caused by the structure after a stress of the same magnitude but in the opposite direction is applied to the newly developed crack surface.

For elements whose integration point does not change before and after the crack propagation, the strain after the n^{th} propagation is

$$\varepsilon_{n+1} = \varepsilon_n + \Delta\varepsilon_n \tag{35}$$

where ε_n is the initial strain at the n^{th} propagation, and

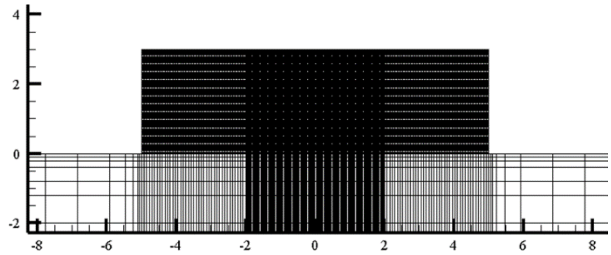

Fig. 9 Computational grid

$\Delta\varepsilon_n$ is the strain increment caused by the structure after a stress of the same magnitude but in the opposite direction is applied to the newly developed crack surface.

For newly developed cracks, the crack tip element prior to crack propagation will become a crack-penetrated element, and some of the conventional elements will become crack-penetrated elements and crack tip elements. For elements whose integration point has changed, the calculations of the stress and strain should be based on the new integration point, the crack tip stress and the progressive strain field.

For an element whose integration point has changed due to crack propagation, the stress of the structure after the n^{th} propagation is

$$\sigma_{n+1} = K_{\text{I},n}\sigma_{\text{mode I},n} + K_{\text{II},n}\sigma_{\text{mode II},n} + \Delta\sigma_n \tag{36}$$

where $K_{\text{I},n}$ and $K_{\text{II},n}$ represent type I and type II stress intensity factors at the n^{th} calculation step, respectively, and $\Delta\sigma_n$ is the stress increment caused by the structure after a stress of the same magnitude but in the opposite direction is applied to the newly developed crack surface.

For an element whose integration point has changed due to crack propagation, the strain of the structure after the n^{th} propagation is

$$\varepsilon_{n+1} = K_{\text{I},n}\varepsilon_{\text{mode I},n} + K_{\text{II},n}\varepsilon_{\text{mode II},n} + \Delta\varepsilon_n \tag{37}$$

where $K_{\text{I},n}$ and $K_{\text{II},n}$ represent type I and type II stress intensity factors at the n^{th} calculation step, respectively, and $\Delta\varepsilon_n$ is the strain increment caused by the structure after a stress of the same magnitude but in the opposite direction is applied to the newly developed crack surface. The meanings of the other parameters in the formula are the same as in Section 2.4.

4. Examples

4.1 Basic information

This paper uses three examples to verify the accuracy and stability of the model. The three examples include the case in which the concrete's elastic modulus is stable but a thermal crack propagates, the case in which the concrete's elastic modulus changes and a thermal crack does not propagate, and the simulation of thermal crack propagation during concrete pouring. The calculation grid is a concrete block 10 m long and 3 m high, as shown in Fig. 9.

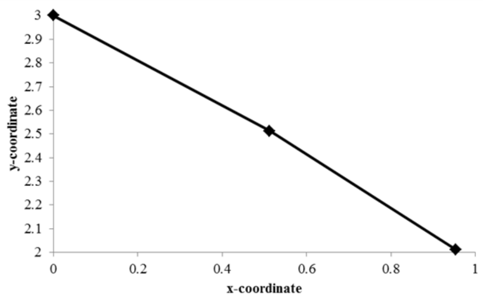

Fig. 10 The initial crack

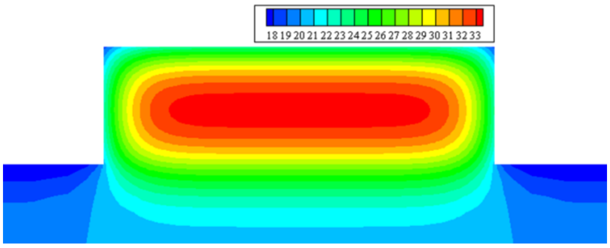

Fig. 11 Final temperatures

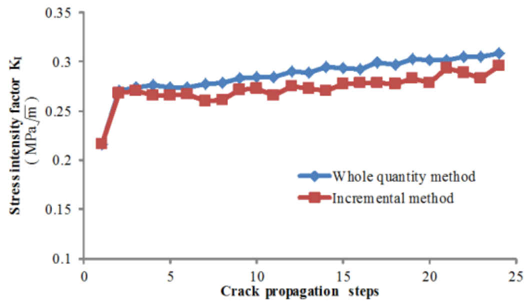

Fig. 12 Development of the stress intensity factor K_I

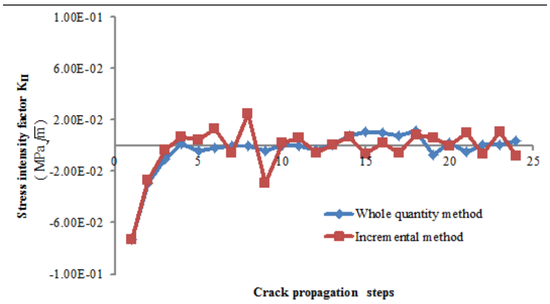

Fig. 13 Development of the stress intensity factor K_{II}

The thermal diffusivity of the concrete is 0.0025 m^2/h, the thermal conductivity is 6.875 kJ/m·h·°C, Poisson's ratio is 0.3, and the linear expansion coefficient of the concrete is 5.5×10^{-6}. The basic thermal diffusivity of the concrete is 0.0033 m^2/h, the basic thermal conductivity is 7.708 kJ/m·h·°C, the basic elastic modulus is 20 GPa, the basic Poisson's ratio is 0.3, and the basic linear expansion coefficient is 5.5×10^{-6}.

4.2 Example of thermal crack propagation

This example studies crack propagation in a concrete block crack with a stable elastic modulus under varying

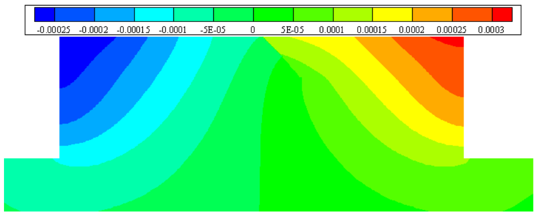

Fig. 14 X-direction displacements obtained by the whole quantity method

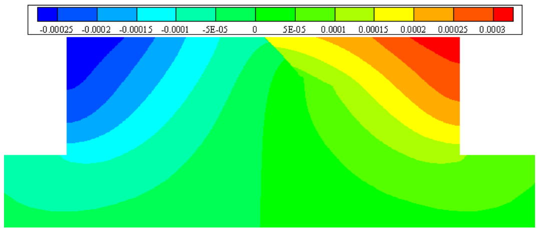

Fig. 15 X-direction displacements obtained by the incremental method

temperature. The elastic modulus of the concrete is 15 GPa, and the model and other material properties are the same as the basic information given in Section 4.1. The position and length of the initial crack are shown in Fig. 10. The initial temperature of the concrete is 20°C, and the final temperatures of the concrete are shown in Fig. 11.

The calculated stress intensity factors are shown in Figs. 12 and 13. The results show that the stress intensity factor K_I increases rapidly and then becomes stable during crack propagation. The stress intensity factor K_{II} decreases rapidly and approaches zero. The results of the incremental method and the whole quantity method are similar; the error is within 5%, and the error did not increase during crack propagation. Fig. 14 and Fig. 15 show the crack propagation displacements at the 25th step. The results show that the displacements obtained using the whole quantity method and the incremental methods are consistent. Thus, the incremental method that was applied in this paper can accurately simulate crack propagation.

4.3 Steady state thermal crack verification example

This example verifies the accuracy of the proposed algorithm in calculating the stress intensity factors for a non-propagated crack. The initial concrete temperature was 20°C, and the external temperature was 25°C. The concrete's adiabatic temperature rise was $\theta = 23(1-e^{-0.4\tau^{0.6}})$ °C, the elastic modulus of the concrete was $E = 3.5(1-e^{-0.25\tau^{0.35}})$ GPa, and the coefficient of heat release of the concrete surface was 6.25 kJ/m^2·h·°C. The model and the other material properties were the same as in Section 4.1. The initial crack was located on the x-direction plane of symmetry of the concrete block (x=0); it was 0.23 m long, and one end was on the concrete surface.

The temperature field distributions of the concrete after 3, 5, and 10 days are shown in Figs. 16, 17 and 18, respectively. The increments in the stress intensity factor during the calculation are shown in Fig. 19. The stress

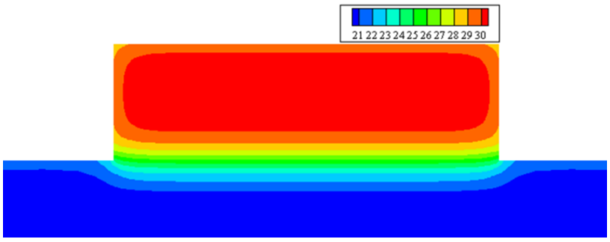

Fig. 16 Temperature distribution in the concrete at day 3

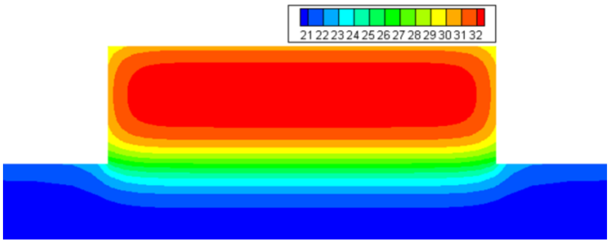

Fig. 17 Temperature distribution in the concrete at day 5

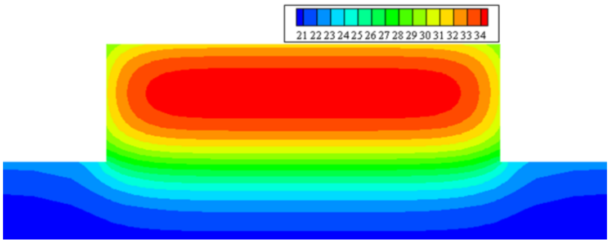

Fig. 18 Temperature distribution in the concrete at day 10

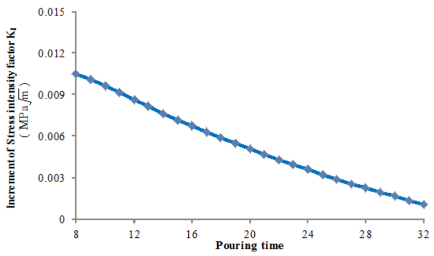

Fig. 19 Increment of the stress intensity factor K_I obtained by the step by step method

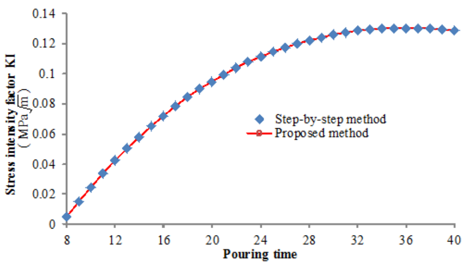

Fig. 20 Development of the stress intensity factor K_I

intensity factors and the difference between the stress intensity factors that were calculated using Eqs. (30)-(33) are shown in Fig. 20. The results show that the stress intensity factors obtained by the two methods are identical.

4.4 Example of thermal crack propagation in hardened concrete

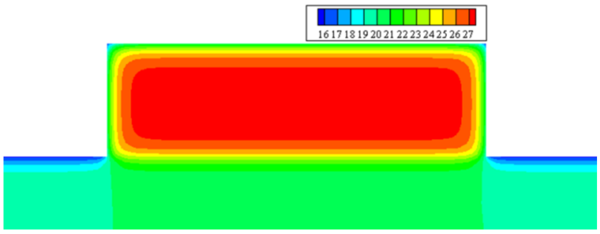

Fig. 21 Temperatures in the concrete on day 1

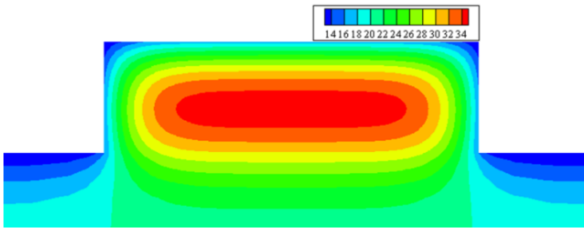

Fig. 22 Temperatures in the concrete on day 10

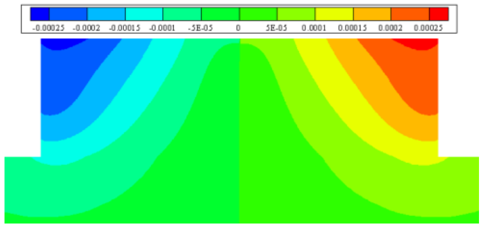

Fig. 23 X-direction displacements in the concrete on day 1

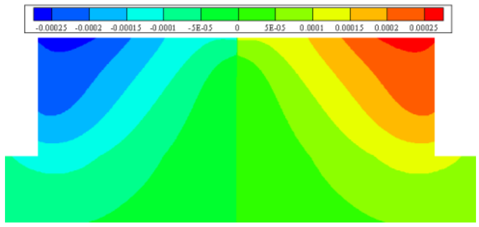

Fig. 24 X-direction displacements in the concrete on day 10

The examples in Sections 4.2 and 4.3 verified the accuracy of the model. This example confirms the stability of the model by studying the displacement variation of a newly poured concrete block during gradual crack propagation. The initial concrete temperature was 20°C, the external temperature was 10°C, the coefficient of heat release of the concrete surface was 20.83 kJ/m^2·h·°C, the concrete's adiabatic temperature rise was $\theta = 23(1-e^{-0.4\tau^{0.6}})$ °C, the elastic modulus of the concrete was $E = 3.5(1-e^{-0.25\tau^{0.35}})$ GPa, and the surface heat release coefficient was 6.25 kJ/ m^2·h·°C. The fracture toughness of concrete is $K_{IC} = 1.5(1-e^{-0.25\tau^{0.35}})\mathrm{Mpa}\sqrt{\mathrm{m}}$.

The model and other material properties were the same as in Section 4.1. The initial crack was located on the x-direction plane of symmetry of the concrete block (where x=0), was 0.175 m long, and one end of the crack was located on the concrete surface.

The temperature field distributions in the concrete after 1 and 10 days are shown in Figs. 21 and 22, respectively, and Figs. 23 and 24 show the calculated displacement distributions. The results show that the displacements are symmetrically distributed, and there are no abnormalities in the calculated results. Clearly, the algorithm has good stability.

5. Conclusions

This paper analyzed two cases of crack propagation in early-age concrete: one in which the crack does not propagate but the elastic modulus of the concrete changes and one in which the crack propagates at a point in time. This paper focused on the characteristics of the extended finite element algorithm when it is applied to these two cases and provided computational models for these two cases. The results show that:

(1) For the case in which cracks do not propagate but the elastic modulus of the concrete changes, this paper presented a method that calculates the strain caused by the elastic stress. This method mainly concentrates on the M integral; therefore, the stress and strain histories are not considered, and the stress intensity factor of the crack can be solved in one calculation.

(2) For the case in which the crack propagates, a stress of the same magnitude but in the opposite direction must be applied to the newly developed crack surface to simulate crack propagation. Based on the stress intensity factor, the analytical solution to the progressive field was applied to fit the stress of the newly developed crack surface.

(3) During the crack propagation process, if the type of element (conventional element, crack-penetrated element or crack tip element) does not change, then the position of the integration point within the element does not change; therefore, the stress and strain can be expressed by a brief superposition. For an element (crack tip element or partial conventional element) whose integration point changes, the analytical solution to the progressive field is used to calculate the stress and strain at the integration point.

The numerical contrast method was applied to verify the accuracy of the proposed model for the case in which the elastic modulus of the concrete is stable but the thermal crack propagates, the case in which the concrete's elastic modulus changes and the thermal crack does not propagate, and the case of thermal crack propagation as well as to verify the stability of the algorithm during the concrete pouring process. The verification results indicate that the method can be used to calculate thermal crack propagation with simple programming. In addition to its advantages of high computational accuracy and stable results, this method can also predict the development of thermal cracks in mass concrete.

Acknowledgements

This research was supported by the National Key Research and Development Project of China (Grant No. 2018YFC0406703), the National Natural Science Foundation of China (Grant No. 51779277, 51579252, 51439005), and the Special Scientific Research Project of the China Institute of Water Resources and Hydropower Research (Grant No. SS0145B392016, SS0145B612017, KY1799).

References

Aliabadi, M.H. (1997), "Boundary element formulations in fracture mechanics", *Appl. Mech. Rev.*, **50**(2), 83-96.

Atluri, S.N. (2002), *The Meshless Local Petrov-Galerkin (MLPG) Method*, Tech Science Press, California, U.S.A.

Belytschko, T., Chen H., Xu J. and Zi, G. (2003), "Dynamic crack propagation based on loss of hypertonicity and a new discontinuous enrichment", *Int. J. Numer. Meth. Eng.*, **58**(12), 1873-1905.

Belytschko T., Lu Y.Y. and Gu L. (1994), "Element-free Galerkin methods", *Int. J. Numer. Meth. Eng.*, **37**(2), 229-256.

Liu W.K., Jun S. and Zhang Y.F. (1995), "Reproducing kernel particle methods in fluids", *Int. J. Numer. Meth. Eng.*, **38**(10), 1655-1679.

Belytschko T. and Black T. (1999), "Elastic crack growth in finite elements with minimal remeshing", *Int. J. Numer. Meth. Eng.*, **45**(5), 601-620.

Bordas S., Rabczuk T. and Zi G. (2008), "Three-dimensional crack initiation, propagation, branching and junction in non-linear materials by an extended meshfree method without asymptotic enrichment", *Eng. Fract. Mech.*, **75**(5), 943-960.

Dong, Y.W. and Ren, Q.W. (2011), "An extended finite element method for modeling hydraulic fracturing in gravity dam", *J. Hydraul. Eng.*, **42**(11), 1361-1367.

Dvorkin, E.N., Cuitino, A.M. and Gioia, G. (2010), "Finite elements with displacement interpolated embedded localization lines insensitive to mesh size and distortions", *Int. J. Numer. Meth. Eng.*, **30**(3), 541-564.

Elena, B. (2014), "XFEM with equivalent eigenstrain for matrix–inclusion interfaces", *Comput. Mech.*, **53**(5), 893-908.

Golebiewska Herrmann, A. and Herrmann, G. (1981), "On energy-release rates for a plan crack", *J. Appl. Mech.*, **48**(3), 525-528.

Himanshu, P. and Akhilendra, S. (2012), "Numerical simulation of bi-material interfacial cracks using EFGM and XFEM", *Int. J. Mech. Mater. Des.*, **8**(1), 9-36.

Jrad, H., Mars, J., Wali, M. and Dammak, F. (2018), "An extended finite element method for modeling elastoplastic FGM plate-shell type structures", *Struct. Eng. Mech.*, **68**(3), 299-312.

Jiang, Y., Tay, T.E., Chen, L. and Sun, X.S. (2013), "An edge-based smoothed XFEM for fracture in composite materials", *Int. J. Fract.*, **179**(1-2), 179-199.

Kim, J.K., Kim, K.H. and Yang, J.H. (2001), "Thermal analysis of hydration heat in concrete structures with pipe-cooling system", *Comput. Struct.*, **79**(2), 163-171.

Linder, C. and Armero, F. (2007), "Finite elements with embedded strong discontinuities for the modeling of failure in solids", *Int. J. Numer. Meth. Eng.*, **72**(12), 1391-1433.

Linder, C. and Armero, F. (2009), "Finite elements with embedded branching", *Fin. Elem. Anal. Des.*, **45**(4), 280-293.

Liu G., Hu Y., Li Q. and Zuo, Z. (2013), "XFEM for thermal crack of massive concrete", *Math. Probl. Eng.*, **12**, 261-294.

Moës, N., Dolvow, J. and Belytschko, T. (1999), "A finite element method for crack growth without remeshing", *Int. J. Numer. Meth. Eng.*, **46**(1), 131-150.

Pan, E. and Yuan, F.G. (2000), "Boundary element analysis of three-dimensional cracks in anisotropic solids", *Int. J. Numer. Meth. Eng.*, **48**(2), 211-237.

Sfantos, G.K. and Aliabadi, M.H. (2007), "Multi-scale boundary element modelling of material degradation and fracture", *Comput. Meth. Appl. M.*, **196**(7), 1310-1329.

Simpson, R.N., Bordas, S.P.A., Trevelyan, J. and Rabczuk, T. (2012), "A two-dimensional isogeometric boundary element method for elastostatic analysis", *Comput. Meth. Appl. M.*, **209-212**(324), 87-100.

Stolarska, M., Chopp, L., Moës, N. and Belytschko, T. (2016), "Modeling crack growth by level sets in the extended finite element method", *Int. J. Numer. Meth. Eng.*, **51**(8), 943-960.

Schutter, G.D. (2002), "Finite element simulation of thermal cracking in massive hardening concrete elements using degree of hydration based material laws", *Comput. Struct.*, **80**(27-30), 2035-2042.

Sneddon, I.N. (1946), "The distribution of stress in the neighborhood of a crack in an elastic solid", *Proc. Roy. Soc. Ser. A*, **187**(1009), 229-260.

Waller, V., D'Aloïa, L., Cussigh, F. and Lecrux, S. (2004), "Using the maturity method in concrete cracking control at early ages", *Cement Concrete Comp.*, **26**(5), 589-599.

Wang, J., Navi, P. and Huet, C. (1997), "Numerical analysis of crack propagation in tension specimens of concrete considered as a 2D multicracked granular composite", *Mater. Struct.*, **30**(1), 11-21.

Wang, J. and Yan, P. (2013), "Evaluation of early age mechanical properties of concrete in real structure", *Comput. Concrete*, **12**(1), 53-64.

Zhu, B.F. (2010), "On pipe cooling of concrete dams", *J. Hydraul. Eng.*, **41**(5), 505-513.

Zhu, Z.Y., Chen, W.M., Qiang, S., Zhang, G.X. and Liu, Y. (2017), "An improvement on the concrete exothermic models considering self-temperature duration", *Comput. Concrete*, **19**(6), 659-666.

Zhu, Z.Y., Qiang, S. and Chen, W.M. (2013), "A new method solving the temperature field of concrete around cooling pipes", *Comput. Concrete*, **11**(5), 441-462.

Zuo, Z., Hu, Y., Li Q.B. and Liu, G. (2015), "An extended finite element method for pipe embedded plane thermal analysis", *Fin. Elem. Anal. Des.*, **102**, 52-64.

Zhu, B.F. (1998), *Thermal Stress and Temperature Control of Mass Concrete*, China Electric Power Press, Beijing, China.

CC